Materials Science & Engineering A 887 (2023) 145717

Contents lists available at ScienceDirect

Materials Science & Engineering A

journal homepage: www.elsevier.com/locate/msea

Order of magnitude increase in actuation fatigue lifetime through partial austenitic transformation of NiTiHf high-temperature shape memory alloys

A. Demblon, J.H. Mabe, I. Karaman *

Department of Materials Science and Engineering, Texas A&M University, College Station, TX, 77843, USA

ARTICLE INFO

Keywords:
High temperature shape memory alloys
Actuation fatigue
Partial transformation
Partial cycling
Minor loops

ABSTRACT

The higher transformation temperatures, strength, and thermomechanical stability of NiTiHf high-temperature shape memory alloys (HTSMAs) are attractive for use in solid-state actuation. Maximizing the actuation fatigue lifetime whilst preventing deterioration of actuation stroke during service are the two main challenges facing the widespread application of HTSMAs. Much research has focused on optimizing composition and processing to enhance performance; however, this has proven challenging to implement on a large scale. Simpler solutions involve optimizing the actuation environment to enhance performance. One of the most effective methods to both extend the lifetime and stabilize actuation strain is through partial thermal cycling. This method is more representative of how actuators are employed, as very rarely are they repeatedly cycled to their maximum output. Previous studies have shown partial transformation extends fatigue lifetime in low-temperature NiTi and NiTiCu SMAs, but it has yet to be conclusively demonstrated in the NiTiHf system. The present work is an extensive analysis of the effects of heating limited partial cycling compared to full cycling actuation fatigue of $Ni_{50.3}Ti_{29.7}Hf_{20}$ HTSMA. The results confirm an order of magnitude increase in actuation fatigue lifetime with less transformation per cycle in partially heated Ni-rich NiTiHf samples. More importantly, keeping the actuation work output almost the same, controlling the actuation strain level is shown to be more effective in increasing the fatigue life than reducing the actuation stress level, yielding 5 to 10 times relative improvement in the fatigue life. The underlying microstructural evolution resulting in the observed enhanced response is provided.

1. Introduction

Shape memory alloys (SMAs) are becoming increasingly well known in a variety of applications due to their shape memory and superelastic effects granted by their unique martensitic transformation properties. Although binary NiTi alloys are by far the most common and thoroughly researched SMAs, NiTiHf high-temperature shape memory alloys (HTSMAs) are being used in an ever-growing array of applications, specifically in the aerospace and automotive industries. The higher transformation temperatures (TTs), strength, and thermomechanical stability of the NiTiHf system are especially attractive for use as active actuators.

Unlike conventional materials, fatigue of SMAs is comprised of structural and functional fatigue. As explained in Ref. [1], structural fatigue is defined by damage accumulation through the formation and growth of cracks which lead to final rupture. Functional fatigue involves the evolution of phase transformation properties such as transformation temperatures, hysteresis, and transformation strains after repeated cycling. As these properties continue to change with cycle number the transformation properties may, at some point, shift outside of the design requirements rendering the SMA device non-functional. Hence, for SMA actuation applications one of the main difficulties facing further implementation is ensuring the actuation fatigue lifetime is sufficiently long to prevent the HTSMA components from being the limiting factor to the service life of a system. Another potential problem for their widespread use is the deterioration of actuation stroke during the lifetime which can be problematic when attempting to have high-fidelity repeatable actuation.

Previous research has shown that one way of solving the aforementioned issues is to optimize the microstructure through careful control of composition, processing, and heat treatments [2–5]. This is, however, complicated due to the extreme sensitivity of transformation characteristics to Ni content in Ni-rich NiTi based SMAs [6–8]. Current research shows that the composition of large-scale productions is

* Corresponding author.
E-mail address: ikaraman@tamu.edu (I. Karaman).

https://doi.org/10.1016/j.msea.2023.145717
Received 1 July 2023; Received in revised form 5 September 2023; Accepted 15 September 2023
Available online 22 September 2023

incredibly difficult to control and there is significant variation from the nominal composition depending on the production methods used and between different manufactured batches [2,9]. Another way to improve actuation fatigue performance is to adjust the actuation conditions, such as load level [10], upper cycle temperature (UCT) [11], heating and cooling rates [12,13], heating current waveform [14], and partial thermal cycling. Partial thermal cycling is defined by heating and cooling the material to temperatures between M_f and A_f such that there is incomplete transformation, i.e. rather than full cycling by heating from $T < M_f$ to $T > A_f$ and cooling back to $T < M_f$, instead, heating from $T < M_f$ to $T < A_f$ or cooling from $T > A_f$ to $T > M_f$, or a combination of these. This method, i.e. partial actuation, is especially pertinent as it eliminates the deterioration of actuation strain amplitude reducing the functional fatigue.

There are relatively few studies on the actuation fatigue of SMAs compared to mechanical fatigue [15–20], let alone partial cycle actuation fatigue of which the authors could only find six studies to date. Of these six studies, three were conducted on binary NiTi, two were on NiTiCu, and only one tested a NiTiHf alloy. Most of the work on NiTi and NiTiCu were performed on thin wires, which, due to processing, can produce different results compared to larger specimens which are better indicators of bulk material response.

Lagoudas et al. [21] and Bertacchini et al. [22] studied the effects of heat treatments, corrosive environment, applied load, and partial transformation cycling on the actuation fatigue life of NiTiCu SMA wires. They found that in $Ni_{40}Ti_{50}Cu_{10}$ (at.%) wire, regardless of the applied load, partial cycling improved the actuation lifetime and the higher the load was the greater the degree to which partial transformation cycling improved the fatigue life. They also demonstrated that the accumulated plastic strain was a function of the number of partial cycles to failure through the Manson-Coffin power-law with a different coefficient, but the same slope, as compared to the full transformation cycles.

Partial actuation cycling of NiTi wires was investigated by Karhu et al. [23] and Mammano et al. [13]. Karhu et al. [23] were primarily concerned with the effects of applied load, heat treatment, and UCT on the actuation response of $Ni_{49.7}Ti_{50.3}$ at. % wire. Their findings were similar to the works performed on bulk NiTiHf HTSMA samples during full actuation cycles [10,11]: higher loads and higher UCT decreased the actuation fatigue life. They demonstrated that during partial transformation cycling, UCT seemed to have a more notable effect than its effect on full cycling, *i.e.*, a 5 °C increase in UCT during partial actuation cycling halved the lifetime, whereas a 40 °C increase in UCT was required to halve the life under full transformation [23]. Mammano et al. [13] performed a very similar study on wires of $Ni_{48.9}Ti_{51.1}$ except they were looking at the effect of heating rate as well as stress and degree of transformation. Here they showed that samples tested to only 80% transformation had nearly 4 times the life with improved functional stability at only a marginal decrease in actuation stroke. However, the microstructural mechanisms responsible for these observations were not clearly revealed in these studies.

A more recent study by Ganesan et al. [24] was focused on partially cycling near equiatomic NiTi dog bone samples to varying degrees and under various loads. Their experiments were not run to failure, but they did demonstrate, similar to the studies mentioned above, that an increase in UCT during partial cycling increases both the amount of recoverable and permanent strain. They also stated that with an UCT nearer the austenite finish (A_f) temperature, there is rapid initiation and growth of cracks and voids. Their explanation for this observation was that more austenitic transformation occurs at higher temperatures, increasing the interfacial area between the transforming phases, which creates more potential crack nucleation sites. However, SEM and TEM results provided were only of the single sample that failed with the highest UCT. No comparative microstructural investigation was conducted to further explain the mechanisms behind the observations due to partial transformation.

The only partial cycle actuation fatigue study on NiTiHf was conducted by Tugrul et al. [25]. They compared partially cycled samples to fully cycled samples under a 200 MPa load on a $Ni_{50.3}Ti_{49.7}Hf_{20}$ alloy. Partially transformed samples were fully cooled to a lower cycle temperature (LCT) and then partially heated until 2% actuation strain was achieved (strain limited). Fully transformed samples were heated from the LCT to a fixed UCT of 300 °C (UCT limited) and had an actuation strain of ~2.5% for the first 1000 cycles before deteriorating. They found no significant difference in actuation fatigue lives between partially cycled and fully cycled samples, however, the partially cycled samples exhibited a greater stability [12,25]. This, somewhat unexpected, observation brings up the question whether partially heating NiTiHf HTSMAs would improve the actuation fatigue life, similar to observations in NiTi and NiTiCu SMAs.

This work seeks to clarify the effects of partial transformation on the actuation fatigue life of a NiTiHf HTSMA by limiting UCT levels to accomplish constant actuation stroke. Additionally, extensive failure analysis is presented to reveal potential differences in microstructural failure mechanisms between fully and partially cycled fatigue specimens.

2. Materials and methods

The NiTiHf HTSMA used for this study had a nominal composition of $Ni_{50.3}Ti_{29.7}Hf_{20}$ (at. %) and was cast via vacuum induction skull melting in a water-cooled Cu hearth. The cast ingots were then homogenized at 1050 °C for 72 h and furnace cooled before being extruded in a steel can at 900 °C to an 8:1 area reduction ratio in one pass. Stress free martensitic transformation temperatures (TTs) and transformation enthalpy were measured using a TA Instruments Q2000 differential scanning calorimeter (DSC) with a heating/cooling rate of 10 °C/min. Samples were tested under two conditions, solution heat treated (solutionized), and as extruded (AE) + aged. DSC on the solution heat treated (precipitate free) samples has been demonstrated to be the most robust indication of actual composition [2] which has been proven to vary from the nominal composition through the many difficulties associated in producing these highly compositionally sensitive NiTiHf alloys [2,6,9]. Solutionizing was carried out at 900 °C for 1 h followed by water quenching with the samples sealed in quartz tubes and backfilled with Ar. The aging heat treatment was conducted at 550 °C for 3 h in air followed by air cooling. This aging treatment was selected based on the previous studies with this material knowing it formed uniform, coherent nanoscale H-phase precipitates resulting in a moderate increase in TTs and high martensitic transformation reversibility [2,3,26,27].

A FEI Quanta 600 scanning electron microscope (SEM) was used to analyze the non-metallic inclusion (NMI) content of the material. A 1.5 mm thick cross section of the 10 mm diameter AE bar was cut via wire electrical discharge machining (EDM) and polished to 1200 grit using SiC sandpaper followed by polishing with a 3 μm diamond slurry. A total of 15 backscattered electron (BSE) images were taken across the sample and analyzed using ImageJ software to calculate the area fraction of the NMIs. Energy dispersive X-ray spectroscopy (EDS) was used to determine the NMI compositions.

Transmission electron microscopy (TEM) was carried out using a FEI Tecnai F20 ST FEG instrument to determine the size and morphology of the H-phase precipitates after aging. TEM foils were prepared by mechanically polishing a 10 mm diameter sample to a thickness of 50–70 μm with a 1200 grit finish before being electropolished. Electropolishing was performed with a solution of 30% nitric acid to 70% methanol by volume at a temperature of −25 °C to −30 °C and a voltage of 11.2 V. Bright-field (BF) images were taken with an accelerating voltage of 200 kV.

Flat actuation fatigue dog bone samples (Fig. 1) with a gage section 40 mm long, 2.5 mm wide, and 1 mm thick were cut using wire EDM and aged at 550 °C - 3 h in air in the as-extruded condition. Actuation fatigue testing was performed using a custom-built experimental apparatus, as

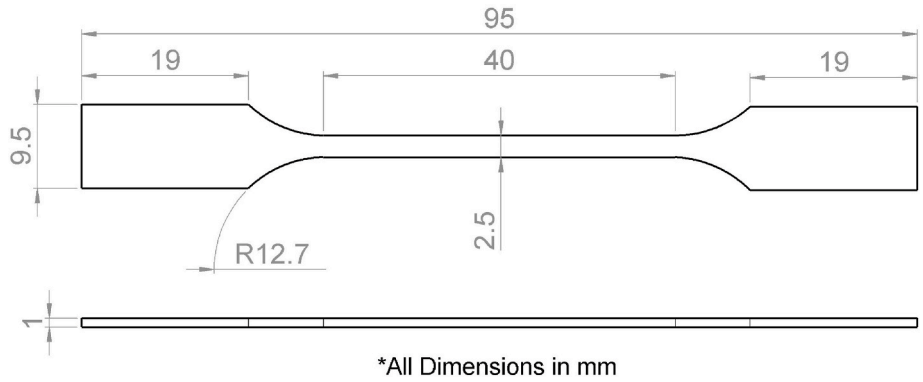

Fig. 1. Top and side view drawing of an actuation fatigue sample used in this work. The dimensions presented are in millimeters.

described in Fig. 2 below. (1) Flat dog bone specimens are clamped in stainless steel friction grips and hung from the frame. (2) Temperature is measured at the center of the gage section using an infra-red thermometer which is mounted perpendicular to the sample and the samples are painted with a flat black high temperature paint to ensure uniform emissivity. (3) An armature connected to the lower grip extends to the linear displacement sensor which measures the extension of the sample during cycling which is converted to transformation strain by dividing by the gage length. (4) A fan is secured to the test frame to convectively cool the sample and can be moved closer or further from the sample to maintain similar cooling rates between tests. (5) A steel cable runs from the bottom grip through the workbench to which weights are hung to achieve the desired load. (6) A variable power supply provides current to joule heat the samples and is adjusted to maintain a constant heating rate. (7) All devices and sensors are written to and read from the National Instruments NI6211 data acquisition device (DAQ). The DAQ connects to a computer where the whole experiment is controlled through custom written LabVIEW code.

During actuation fatigue testing samples are loaded to a constant force and thermally cycled; generating data in the form of strain/temperature hysteresis loops as the material undergoes phase transformation. The idealized strain vs. temperature diagram in Fig. 3 illustrates how the full and partial transformation fatigue tests were performed. One full actuation cycle is defined by cooling from the UCT to the LCT and heating back to the UCT, depicted by the dashed blue and red lines, respectively. A partial heating cycle is defined by heating up from the LCT to the partial heating UCT (PHUCT) and cooling back to the LCT, drawn in solid red and blue lines. The strain under load at the UCT is the UCT strain (ε_{UCT}) and the strain at the LCT (below M_f) is the LCT strain (ε_{LCT}). A partial strain value (ε_{par}) is defined as the strain at the PHUCT during incomplete thermal cycles. The UCT strain value upon initial loading, before any thermal cycling, is the reference strain (0% strain). Actuation strain is defined as the difference between ε_{LCT} and ε_{UCT} or ε_{LCT} and ε_{par}, during reverse transformation (LCT to UCT or PHUCT), for full cycling or partial cycling, correspondingly.

All samples were loaded to a constant force yielding an initial stress of 300 MPa and tested to four levels of transformation: 100–0% martensite volume fraction (MVF), 100–10% MVF, 100–25% MVF, and 100–50% MVF. Full transformation (100–0% MVF) cycles were performed by cycling the sample between a LCT of 35 °C and UCT of 300 °C. The partial cycling tests were run for 100 cycles under full transformation to move into stabilized actuation regime and determine the maximum attainable actuation strain. After 100 cycles the samples were cooled to the LCT and only heated until the desired fraction of maximum actuation strain was reached (i.e. $\varepsilon_{act,par} = 90\%$, 75% or 50% of ε_{act}). The average joule heating and convective cooling rates for full cycling (35 °C → 300 °C → 35 °C) were 15.8 ± 1.6 °C/s and 7.0 ± 0.5 °C/s, whereas the average heating and cooling rates for partial cycling (35 °C → X °C → 35 °C) were 19.3 ± 3.9 °C/s and 4.0 ± 0.6 °C/s respectively. The heating rate for partial cycling is higher as the PHUCT is lower than the full cycling UCT thus with the same voltage heating is faster. The partial cycling cooling rate is lower than that under full cycling due to a lower sample temperature at the PHUCT than the UCT as dictated by Newton's law of cooling which proves the amount of heat transferred is proportional to the temperature difference between the sample and surrounding fluid. At least three repetitions were conducted under each

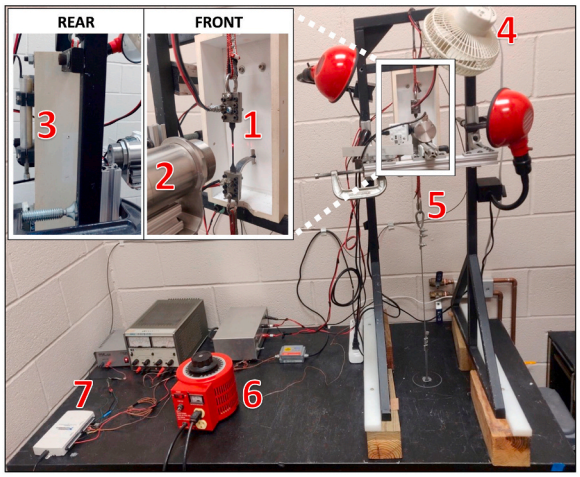

1. Clamped Sample
2. Infra-red Thermometer
3. Linear Displacement Sensor
4. Fan
5. Cable to Load
6. Joule Heating Power Supply
7. Data Acquisition Device

Fig. 2. Custom experimental setup used for the actuation fatigue tests in this study. The major components are marked with red numbers which correspond with the labels to the right of the figure. (For interpretation of the references to color in this figure legend, the reader is referred to the Web version of this article.)

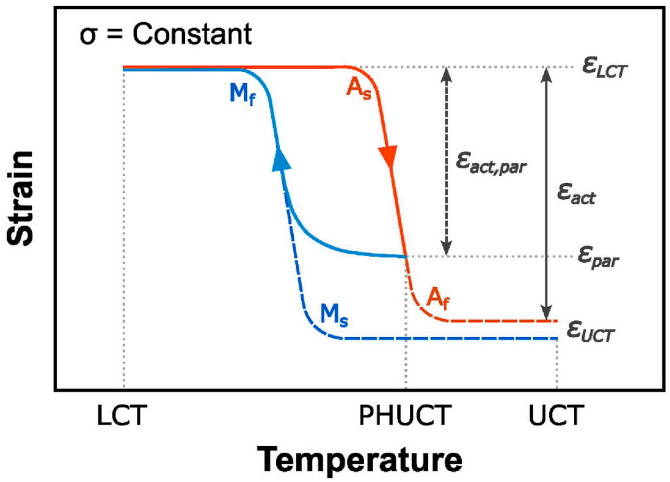

Fig. 3. Schematic of a typical strain vs. temperature plot for SMAs under a constant force. The blue lines correspond to cooling from austenite to martensite and the red lines correspond to heating from martensite to austenite. The dashed lines are representative of full cycling between a lower cycle temperature (LCT) and an upper cycle temperature (UCT). The solid lines represent a partial heating cycle, heating from the LCT to a partial heating UCT (PHUCT) until the desired fraction of actuation is attained. M_f, M_s, A_s, and A_f correspond to the transformation temperatures at the applied load σ. E_{LCT}, ε_{UCT}, and ε_{par} mark the LCT strain, UCT strain, and partial heating strain (strain at the PHUCT) attained during thermal cycling under load. The actuation strain during full cycling and partial cycling (ε_{act} and $\varepsilon_{act,par}$, respectively) are calculated as the difference between the strain at the LCT and the UCT or PHUCT during heating. (For interpretation of the references to color in this figure legend, the reader is referred to the Web version of this article.)

condition except for the 100–50% MVF case where only one test was run due to the costly amount of time it took the sample to fail.

Post-mortem analysis was performed using a macro photographic lens and secondary electron (SE) imaging of the fracture surfaces. Gage section segments of 5 mm adjacent to the crack surface were carefully polished to the same depth with a 1200 grit finish and optical microscopy (OM) was used to image the surface cracks present in the failed samples.

3. Experimental results

3.1. Thermal and microstructural characterization

To thoroughly characterize the material used in this study, the nominal $Ni_{50.3}Ti_{29.7}Hf_{20}$ HTSMA was screened for transformation temperatures, impurities, and H-phase precipitate content after aging. These properties provide valuable input as to the type of response that may be seen as well as determining the SMA transformation characteristics which are paramount when designing boundary conditions for the fatigue experiments. In addition, it is the authors' opinion that presenting the impurity content and H-phase size and morphology allows a more accurate result comparison of any further studies on this material.

Transformation temperatures (TTs) of the NiTiHf alloy were determined using the DSC curves shown in Fig. 4 following the ASTM F-2004-17 standard [28]. The martensite finish (M_f), martensite start (M_s), austenite start (A_s), and A_f temperatures of the solutionized (precipitate free) samples were 44 °C, 54 °C, 89 °C, and 103 °C, respectively. Aging at 550 °C – 3 h increased TTs to a M_f of 104 °C, M_s of 119 °C, A_s of 140 °C, and A_f of 155 °C. This was an increase of ~60 °C to the martensite temperatures and ~50 °C increase to the austenite temperatures as compared to the precipitate free condition. The thermal hysteresis (A_f – M_s) in the aged material was 36 °C which was lower than the 49 °C hysteresis in the solutionized material.

The detrimental effect of inclusions and cleanliness on the structural

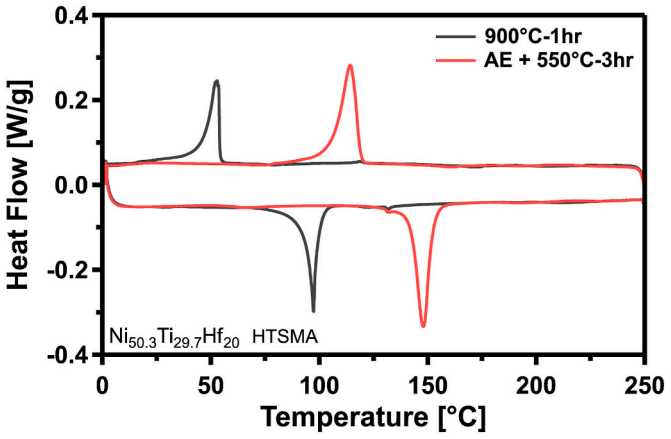

Fig. 4. Differential Scanning Calorimetry (DSC) results of the $Ni_{50.3}Ti_{29.7}Hf_{20}$ alloy in this study showing the transformation temperatures of the solutionized and as extruded (AE) + aged conditions. The solution heat treatment was 900 °C – 1h, and the aging treatment was 550 °C – 3h.

fatigue life of NiTi SMAs has been thoroughly documented by Rahim et al. [29]. There are two types of oxides present in this material as evidenced by the back scattered electron (BSE) images of the AE material shown in Fig. 5a. EDS analysis proved the bright white particles to be HfO_2 and the black particles to be $(Ti + Hf)_4Ni_2O_x$. The average area fraction of all oxides was calculated to be 0.17 ± 0.03% with an average area per particle of 0.8 ± 0.2 μm^2. These results show that this material can be considered very "clean" based on a recent comparative study involving the effects of oxide NMI content on the actuation fatigue lives as well as the 0.17% NMI area fraction being an order of magnitude lower than the ASTM F2063 limit of 2.8% [2,30]. The Bright Field (BF) TEM images show the H-phase precipitates to be small and densely and evenly distributed after aging at 550 °C for 3 h (Fig. 5b). Examination of these precipitates yielded an average length of 11.7 ± 3.0 nm, and an average width of 6.9 ± 1.8 nm.

3.2. Actuation fatigue response

After characterizing the material, partial cycle actuation fatigue tests were conducted under a fixed load of 300 MPa to the four previously stated degrees of transformation, 100-0% MVF, 100-10% MVF, 100-25% MVF, and 100-50% MVF (which correspond to 100%, 90%, 75%, and 50% of full transformation). As was shown in Fig. 3 the strain vs. temperature data is crucial in analysing actuation performance. This data not only illustrates how the austenite, martensite, and actuation strains evolve over the life of the sample, but it shows how transformation temperatures and hysteresis change with an increasing number of cycles.

Representative strain vs. temperature responses for each condition are shown in Fig. 6 below. The grey lines show the first 100 control cycles which were run between a fixed LCT and UCT. The stacked light blue lines are the remaining cycles until failure i.e., from the LCT to UCT for 100% transformation and from LCT to the PHUCT for <100% transformation. The 101th cycle (shown in black) is the first true cycle at each test condition as it is the first cycle after the 100 control cycles. The red line is the last complete cycle before the sample ruptures. In all four figures the curves shift up and to the right in small increments with each cycle. The curves shifting up indicates an increase in inelastic deformation causing the sample to elongate over time. The evolution of strains associated with this upward shift is better visualized in Fig. 7 and is addressed below. The shifting to the right is from the increase in PHUCT over time which suggests that a higher driving force is required to attain the same degree of transformation as the specimens undergo further repeated transformation. At the start of partial cycling, PHUCTs

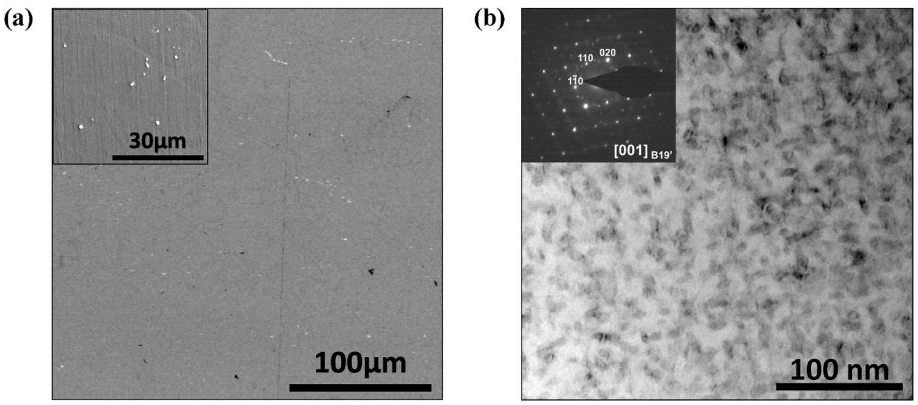

Fig. 5. SEM and TEM images of the $Ni_{50.3}Ti_{29.7}Hf_{20}$ HTSMA used in this investigation. (a) Backscattered electron (BSE) image of the as extruded (AE) material, showing white HfO_2 and black $(Ti + Hf)_4Ni_2O_x$ particles in the grey NiTiHf matrix. (b) Bright-field (BF) TEM image and selected area electron diffraction (SAED) pattern showing the H-phase precipitate content after the 550 °C – 3h aging heat treatment.

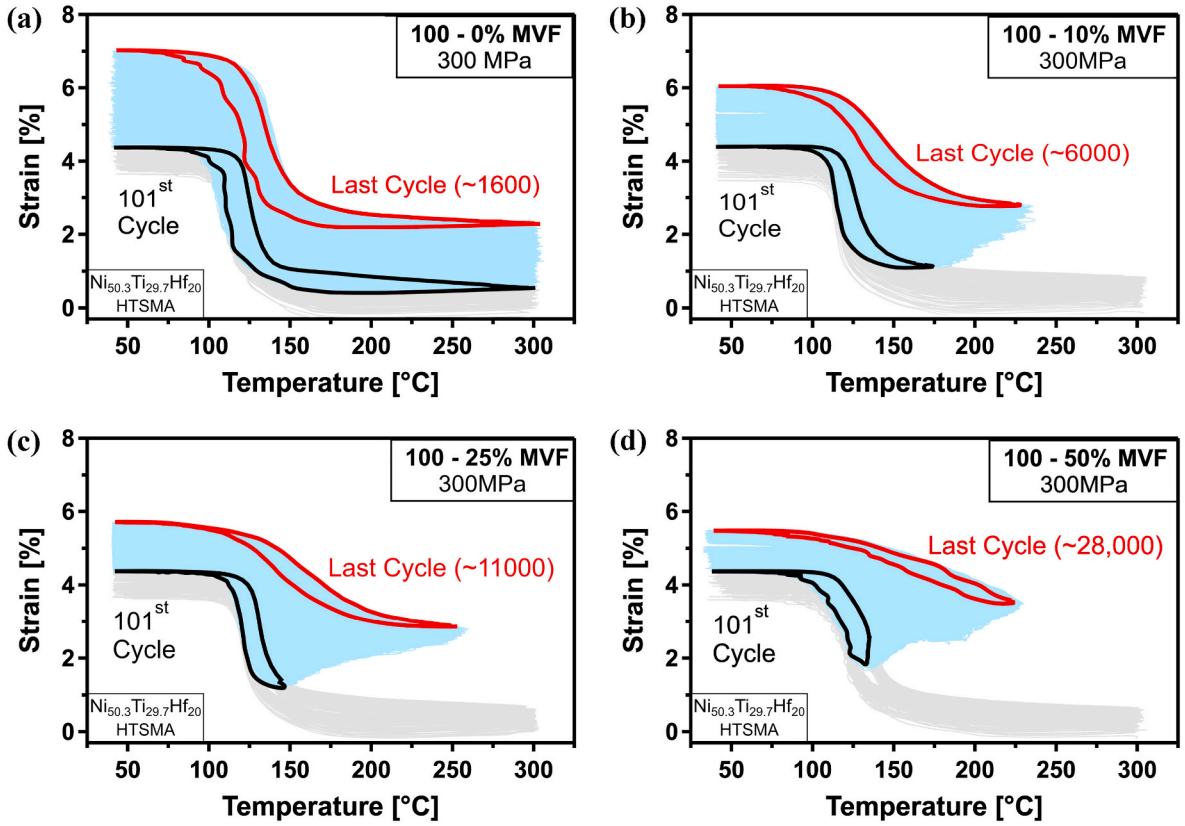

Fig. 6. Strain vs. temperature responses of the $Ni_{50.3}Ti_{29.7}Hf_{20}$ actuation fatigue samples conducted under 300 MPa to a transformation of 100–0% MVF, 100-10% MVF, 100-25% MVF, and 100-50% MVF 100 full transformation control cycles. The grey curves are the 100 control cycles, the blue curves are all the partial cycles, the black curve is the 101th cycle (the first partial cycle), and the red curve is the last full cycle before failure. The last cycle number is an average of all tests run at that condition rounded to the nearest 100 cycles. (For interpretation of the references to color in this figure legend, the reader is referred to the Web version of this article.)

of 175 ± 9 °C, 148 ± 7 °C, and 133 ± 11 °C were required to attain 90%, 75%, and 50% transformation respectively. Near failure, higher temperatures of 235 ± 11 °C, 260 ± 8 °C, and 230 ± 9 °C, respectively, were needed to attain those same degrees of actuation. From the strain vs. temperature responses, it can be seen that there was no significant change in hysteresis width from the first to the last cycle in any case. This implies that the microstructural changes that occur during actuation fatigue do not change the amount of energy dissipation during the partial phase transformation.

The evolution of actuation strain and LCT strain over lifetime derived from the strain/temperature data is provided in Fig. 7, where actuation strain is calculated as the difference between the LCT strain and UCT strain during the heating portion of the cycle. It is easy to see that the higher the degree of partial transformation the greater the fatigue life at the expense of actuation strain. The evolution of irrecoverable strain (UCT strain) is not displayed because under partial transformation the samples are not fully heated to austenite, thus, the results would be misleading. The actuation strain after the 100 control cycles is ~4%, thus, making the target actuation strains for the 100–10%, 100–25%, and 100–50% partial cycle conditions ~3.6%, ~3%, and ~2%

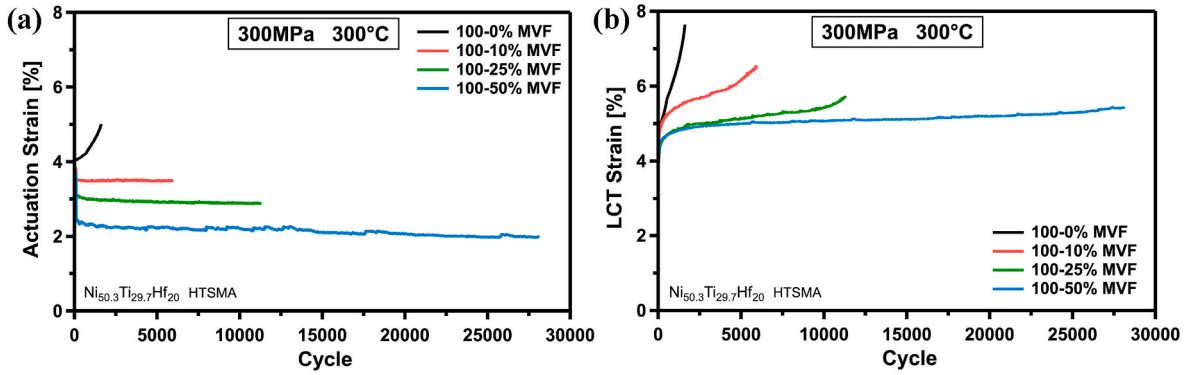

Fig. 7. The evolution of (a) actuation strain, (b) lower cycle temperature (LCT) strain evolution to actuation fatigue failure of the AE + aged $Ni_{50.3}Ti_{29.7}Hf_{20}$ HTSMA samples tested at 300 MPa to 100%, 90%, 75%, and 50% of actuation.

respectively. Fig. 7a shows the actuation strain of the 100–0% MVF sample increasing with cycle number, and the actuation strain of the three partial cycle conditions remaining stable. This is because the fully cycled sample was tested under temperature control whereas the partially cycled tests were conducted under strain control. Strain control ends the heating cycle when the fixed target actuation strain is reached so the actuation strain should remain constant at the targeted value. However, there is a very slight negative slope to the 100–25% and 100–50% MVF samples due to the A_s to A_f transformation regime having a steep negative gradient near the beginning of the test and shallowing out after further cycling (as can evidenced in Fig. 6 above). With a steep transformation gradient, any small overshoot in temperature (of even a couple of degrees) due to the minor delay between heating and cooling cycles results in a slightly higher actuation strain than was targeted. This effect is less pronounced with the shallower transformation gradient present in later cycles.

The fully cycled sample survived only 1483 ± 194 cycles with an initial actuation strain of 3.7 ± 0.3% and failing at an actuation strain of 4.5 ± 0.4%. Less transformation greatly increased the fatigue life with the 90%, 75%, and 50% transformed samples lasting 5630 ± 1278 cycles, 13,009 ± 2575 cycles, and 28,102 cycles, respectively. At 50% actuation the fatigue life was extended nearly 19 times that of the fully cycled samples. Interestingly, lower transformation fraction also lowered the value and rate of increase in LCT strain. Under 100–0% MVF the LCT strain was 7.6% at failure followed by 6.6%, 5.7%, and 5.6% LCT strain at failure for the subsequent partial cycle conditions in reducing degree of transformation.

3.3. Post-mortem analysis

The fractography investigation was conducted via SEM and OM and was centered on observing the cracks that formed on the free surfaces during thermomechanical cycling, as well as examining the fracture surfaces themselves. In order to perform these analyses a 5 mm long section adjacent to the fracture surface on one half of the failed sample for each condition was cut and carefully polished to the same depth to reveal the surface cracks. Fig. 8 below shows most of these surface cracks are clustered to the edges of the sample and these edge cracks are significantly longer than any interior cracks. The 100–0% MVF sample clearly has more cracking on the edge and interior with a greater crack tortuosity of the fracture surface itself compared to all other cases. The sample cycled to 75% transformation seems to have the next highest amount of cracking followed by the 100–10% MVF and lastly the 100–50% MVF samples. It should be noted that although it is difficult to

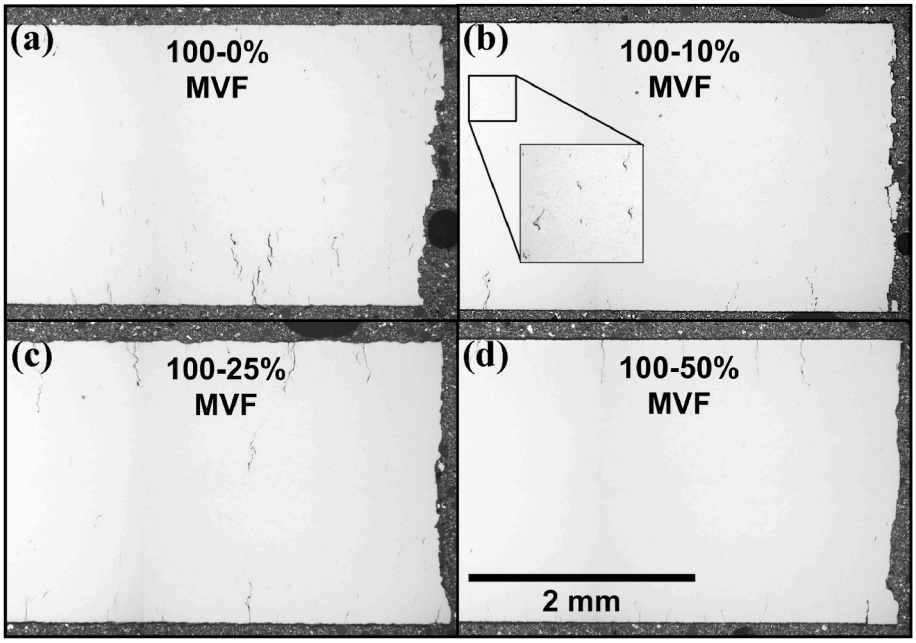

Fig. 8. Optical microscopy images of the surface cracks in failed actuation fatigue samples of $Ni_{50.3}Ti_{29.7}Hf_{20}$ HTSMA adjacent to the fracture surface for each test condition conducted at 300 MPa; (a) 100–0% MVF, (b) 100–10% MVF, (c) 100–25% MVF, and (d) 100–50% MVF.

see the interior cracks at this magnification, if zoomed in (inset of Fig. 8b) there are many small interior cracks in the 90% partially cycled samples. The images in Fig. 8c and d do not have interior damage to the same extent. 100–0% and 100–10% MVF samples exhibit a notably higher fraction of interior cracks than 100–25% and 100–50% MVF samples, while the latter two feature longer edge cracks than the former.

Fracture surface analysis was conducted primarily via SE imaging in the SEM. In addition, a macro camera lens was used to take a photograph of the fracture surfaces to see the heat tinting denoting the crack propagation area before rupture (Fig. 9). This discoloration is due to the surface oxidation in air when thermally cycled above 200 °C during the actuation fatigue test. It is unlikely that any free surface oxidation of the crack has any significant effect on the actuation fatigue response. The fracture surface imaging results summarized in Fig. 9 and clearly display three fatigue fracture regions: initiation, propagation, and rupture. Fig. 9(**i**) shows that for all conditions the crack propagation that led to final rupture was caused primarily by a crack that initiated at a surface. Interestingly, the crack propagation surface area is inversely related to fraction of transformation. The propagation region of the fully cycled sample reached only ~20% of the total fracture surface area, whereas samples cycled to only 75% and 50% of actuation had propagation regions covering ~22% and ~31% of the cross section, respectively. The 90% actuation sample differed from the other samples in that the main crack propagation region was only to ~17% of the total fracture surface area which is less than that of the fully cycled sample. However, there are other oxidised areas visible away from the main crack showing different cracks propagating before rupture. This results in a total propagation region greater than the primary crack surface area of ~17%. Regardless, it proves the crack propagation rate is drastically reduced by partial heating actuation cycling as it took nearly four times the number of cycles for the crack to propagate to a similar extent as a fully cycled sample.

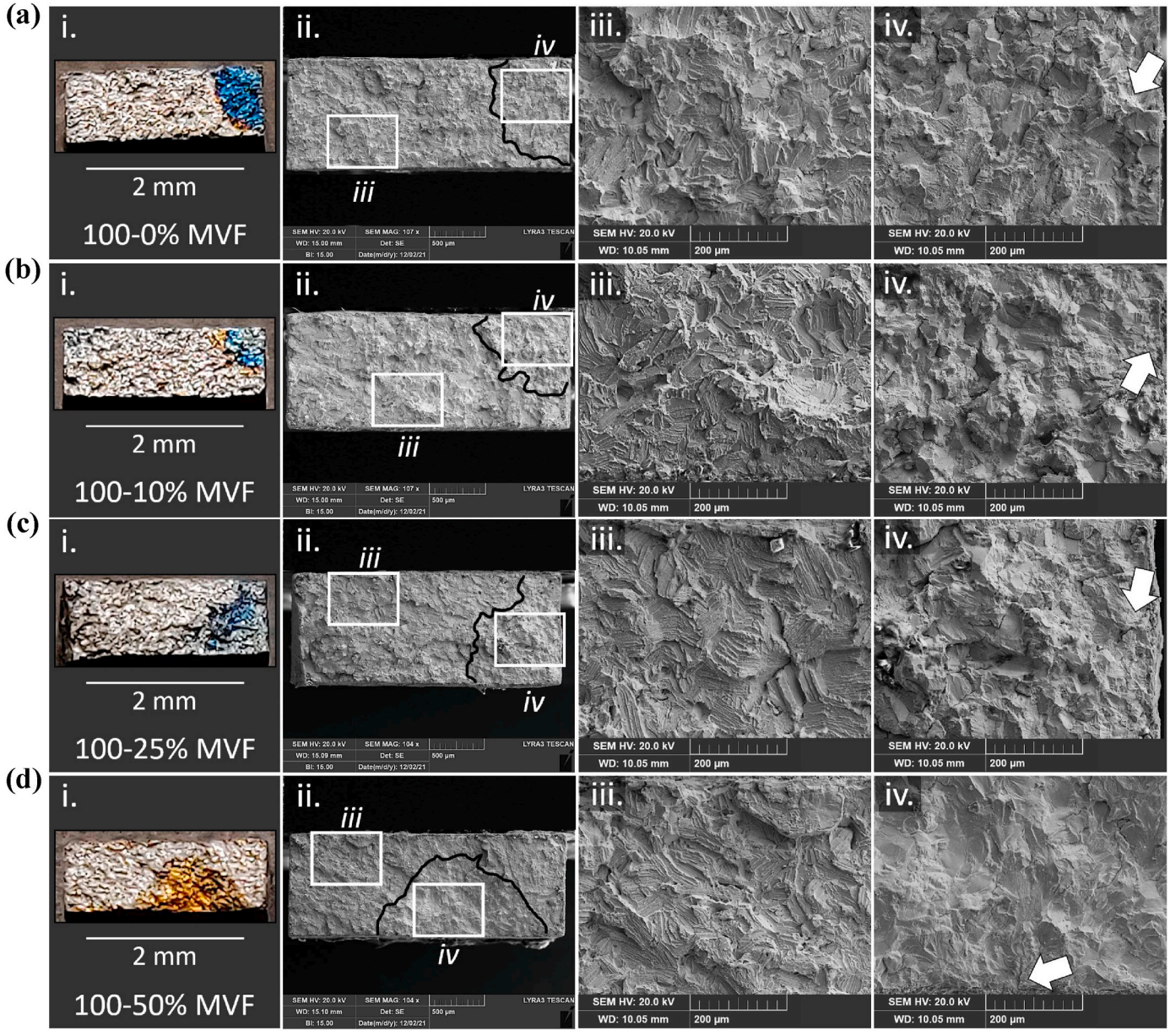

Fig. 9. Actuation fatigue fracture surface analysis of the NiTiHf samples failed after testing to 100%, 90%, 75%, and 50% of transformation under 300 MPa. (a) displays the fracture surface tested to 100% actuation transformation (100–0% MVF), (b), (c) and (d) present the fracture surfaces for 100–10% MVF, 100–25% MVF and 100–50% MVF samples accordingly. The columns of images increase in magnification from i to iv, with iii and iv being at the same magnification. (iii) is a zoomed in area of the fracture surface that underwent rupture, and (iv) is focused on the crack initiation and propagation zone.

The appearance of the fracture surfaces was similar regardless of whether the samples were fully or partially cycled. The crack initiation site, marked with a white arrow (Fig. 9 (iv)), is revealed by the typical river marks emanating from the initiation zone. The initiation sites appear to have undergone primarily transgranular cleavage with a relatively smooth fracture surface. With lower levels of actuation, the crack propagation regimes become increasingly transgranular, whereas fully transforming samples are dominated by intergranular fracture. The final rupture zone was predominantly transgranular revealing a patchwork of lines that appear to be martensite lathes (Fig. 9 (iii)) but there are interspersed regions of intergranular fracture. Although the rupture zones have a combination of transgranular and intergranular cracking, the higher the degree of transformation (i.e., 100–0% MVF), the more intergranular fracture is present.

4. Discussion of the results

From the many results presented it may be challenging to understand if or how these results aid in understanding any differences observed between full and partially heated actuation fatigue experiments. This section focuses on comparing the differences observed between full and partial cycling and discussing the probable causes. Section 4.1 focuses on extracting more information from the actuation fatigue results provided in section 3.2. Section 4.2 focuses on the post-mortem analysis given in 3.3 and how this evidence relates to the fatigue results. Section 4.3 presents the underlying mechanisms in effect during partial cycling as compared to full cycling.

4.1. Comparison of the effects of partial and full transformation cycling on actuation fatigue response

It is clear from the above results that partial heating can increase the fatigue lifetime by an order of magnitude. It is not clear, however, if this increase in lifetime follows a trend with decreasing actuation strain. Hence, Fig. 10 was plotted relating actuation fatigue lifetime to average actuation strain per cycle. There is a non-linear decrease in lifetime with increasing actuation strain and it can be fit with a polynomial trendline. Although, it may be a linear relationship between the degrees of partially cycled samples which then breaks down in the fully cycled regime where the effect of UCT and other factors begin to dominate as degree of transformation is no longer a factor. It should be noted that the 100–0% MVF samples, cycled from the LCT to the UCT from start until failure survived 1483 ± 194 cycles had a starting actuation strain of 3.7 ± 0.3% and final actuation strain of 4.5 ± 0.4%. This large and rapid increase in actuation strain is thought not to be the true “strain” but rather an apparent strain due to extensive formation of microcracks which open and close (during cooling and heating correspondingly) causing a pseudo actuation strain increase [11].

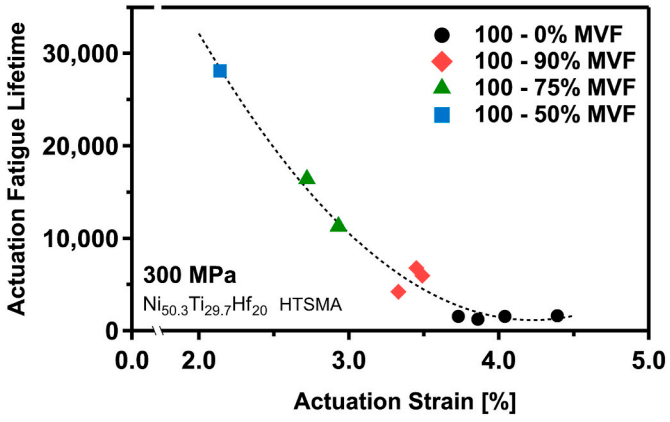

Fig. 10. Scatter plot of actuation fatigue lifetime vs. average actuation strain after the 100 full cycle control cycles of all $Ni_{50.3}Ti_{29.7}Hf_{20}$ HTSMA samples tested. The polynomial trendline indicates the non-linearity of the trend in decreasing fatigue life with increasing actuation strain.

To ensure the observed trend of decreasing lifetime with increasing actuation strain was due to partial transformation and not just a factor of actuation strain magnitude (which can be altered by varying loads with a constant UCT). Additional experiments were carried out on the same material with a fixed UCT of 300 °C and applied stresses ranging from 150 MPa to 450 MPa. Fig. 11 compares the distinct effects of partial cycling and varying loads on actuation fatigue lifetime. Fig. 11a shows the average work output vs. lifetime where the work output is calculated as applied load (σ) in MPa multiplied by the actuation strain (ε_{act}) for each cycle and then averaged. This figure clearly proves that small decreases in useful work through partial transformation results in great increases in service life; significantly more so than producing similar reduced work output by lessening applied stress. This figure also demonstrates a clear difference in trend when increasing the actuation lifetime by reducing work output through applied stress reduction or partial cycling.

The evolution of LCT strain portrayed in Fig. 7b was expanded to include the LCT strain evolution of fully cycled samples under varying loads (Fig. 11b). This figure elucidates some of the reasoning behind the increased lifetime during partial cycling compared to the fully cycled samples under lower stresses. In both fully transformed and partially transformed samples a faster increase in the LCT strain level results in decreasing lifetime. Thus, the swifter accumulation of martensite with a greater degree of transformation (as with a greater applied stress) indicates a more rapid accumulation of damage, likely a combination of transformation induced plasticity (TRIP) and microcrack nucleation and growth. Clearly partial heating retards this damage accumulation significantly more than is possible through load reduction.

It is unlikely that there is any viscoplastic contribution to either the fully or partially transformed samples with the highest cycling temperature being only 300 °C, which is significantly lower than 30–50% of the melting temperature where viscoplasticity in metals starts to occur [31]. With a lower fraction of transformation, it appears there is less overall damage in the material as well as slower damage accumulation as indicated by the rate of increase in LCT strain. It is logical to assume that as there is less global phase transformation occurring during partial cycling, generating less TRIP, reducing stress concentrations due to plastic slip and in turn reducing the propensity of crack nucleation (Figs. 8 and 9).

Another indication of increased defect generation during repeated transformation is the rise in the PHUCT to attain the same actuation strain with increasing cycle number, as seen in Fig. 12a. The average increase in PHUCT for the 100–10% MVF, 100–25% MVF, and 100–50% MVF conditions were 62 ± 9 °C, 114 ± 8 °C, and 97 ± 10 °C, respectively. There does not seem to be an obvious relation between the magnitude of PHUCT increase and degree of transformation. Specifically as the ΔPHUCT for the 75% and 50% actuation are not significantly different with similar values within error. However, there is a clear decline in the rate of PHUCT increase with a lower degree of transformation with an average rate of 0.011 °C/cycle, 0.009 °C/cycle, and 0.003 °C/cycle for 90%, 75%, and 50% transformation, correspondingly. This reiterates the lower rate of TRIP and damage generation with a reduced fraction of transformation as PHUCT only increases to overcome barriers to transformation produced by TRIP and damage accumulation.

The trends in M_f and A_s temperatures during cyclic evolution, as in Fig. 12b, appear mostly similar, i.e. when M_f increases so does A_s. Under full transformation cycling, the TTs decrease until roughly a third of the lifetime and then rise until failure. The 100–10% MVF condition show a small increase in both M_f and A_s. For 100–25% MVF there is only a slight increase in M_f but A_s decreases at first and then increases after ~5000 cycles. The 100–50% MVF condition displayed a reverse trend, where M_f and A_s increase for the first third of the life and then decrease, with A_s

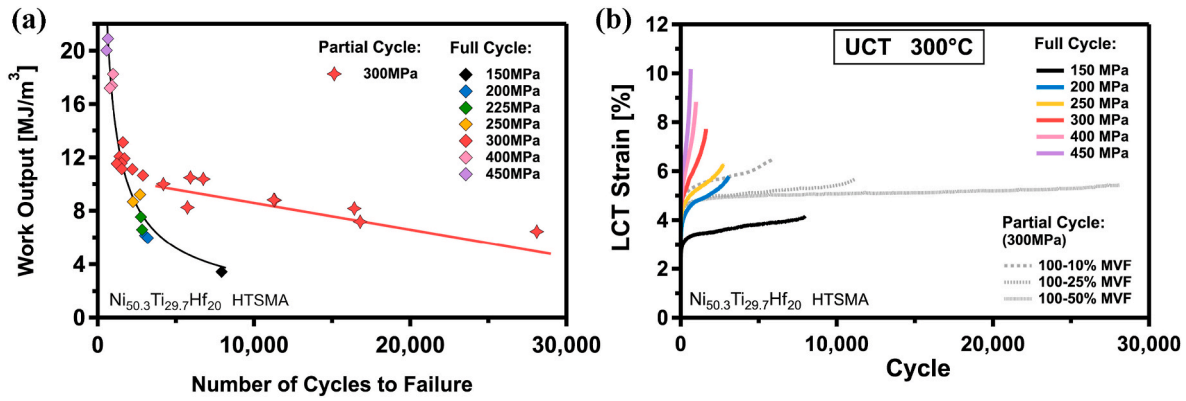

Fig. 11. (a) Work output ($\sigma \cdot \varepsilon_{act}$) vs. number of actuation cycles to failure and (b) lower cycle temperature (LCT) strain evolution for $Ni_{50.3}Ti_{29.7}Hf_{20}$ HTSMA samples showing the distinct effects of partial cycling and applied stress on the actuation fatigue lifetime. Fully cycled samples were loaded between 150 MPa and 450 MPa with a constant upper cycle temperature (UCT) of 300 °C. Partially cycled samples were loaded to 300 MPa and cycled to 90%, 75%, or 50% of full transformation varying UCT to attain a fixed actuation strain.

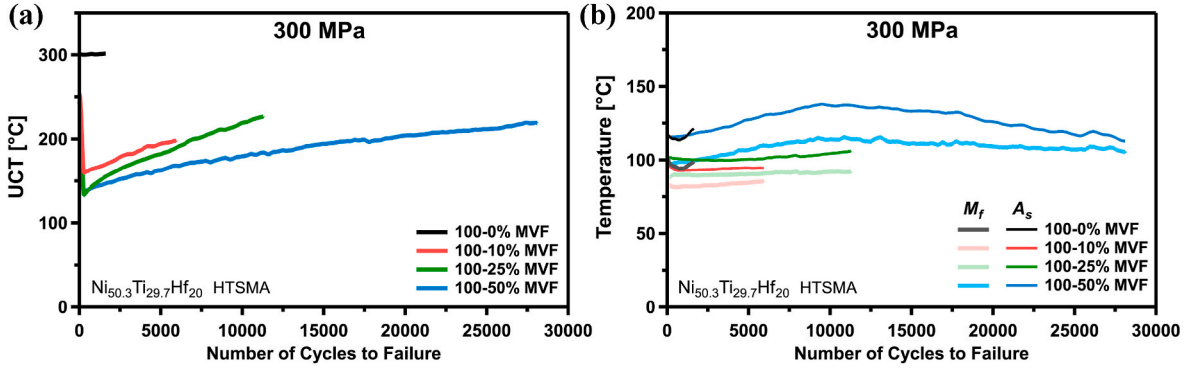

Fig. 12. Evolution of upper cycle temperature (a) and transformation temperatures (b) with cycle number during actuation fatigue testing of $Ni_{50.3}Ti_{29.7}Hf_{20}$ HTSMA samples. Only the M_f and A_s transformation temperature evolutions are *displayed* in (b) due to partial heating not yielding a true M_s and A_f temperature. The data in these figures was generated using the ASMADA tool developed by Kuner et al. [32].

decreasing at a greater rate than M_f. A decrease in M_f can indicate the forward (Austenite (A) – Martensite (M)) transformation is becoming more difficult, and vice versa for increasing M_f. Conversely, lower A_s can indicate the M-A transformation is becoming easier, or more difficult for increasing A_s.

Such an evolution of transformation temperatures indicates that for full actuation cycling, during the first several hundred cycles, dislocations accompanying phase transformation are randomly distributed, they act as a barrier against martensitic transformation and increase the stored elastic strain energy in the martensite phase. This increase in stored elastic strain energy delays the completion of A-M transformation, requiring more undercooling for completion as revealed by the lowering M_f. This also causes the observed decrease in A_s as the necessary M-A driving force is reduced by the higher LCT strain energy. After additional cycling, dislocation substructures start to form generating oriented internal stresses which stabilize martensite and increase all transformation temperatures including M_f and A_s. For 90% and 75% partially cycled samples there is no significant variation observed due to the existence of dislocation "free" regions available for transformation as damage only accumulates in previously transforming regions.

The reverse trend in the 100–50% MVF sample suggests a slightly different mechanism. The increase in M_f and A_s with the number of cycles is from dislocation generation being very localized in the transforming regions, leading to oriented internal stress similar to what is observed in NiTi during actuation cycling [33], in particular near grain boundaries, triple junctions and at the boundary between transforming and non-transforming regions, leading to overall increase in all transformation temperatures. The subsequent decrease in the transformation temperatures during the second half of life indicates the driving force for transformation is lowered as the grain interiors begin transformation allowing the creation of more uniform and randomly distributed dislocations, hindering the completion of the transformation nearer the center of the grains.

4.2. Crack initiation, propagation, and rupture

The surface crack images (Fig. 8) show that there was more damage in the fully cycled samples compared to the partially cycled samples, as expected. Although there seems to be more cracking in the 100–25% MVF samples compared to the 100–10% MVF samples, this may be due to the fact that the former survived twice as many cycles to failure. However, there are less internal cracks with less transformation, regardless of the samples lasting more cycles. Furthermore, the edge cracks of the partially cycled samples are less tortuous and don't branch off the main cracks as much as the fully cycled samples demonstrating a slower and more controlled crack propagation. After initial OM imaging the polished surface crack samples were thermally etched to reveal the grains. Fig. 13 displays a representative comparison between full and partial cycling crack formation by comparing the 100–0% MVF (Figs. 13a) and 100–50% MVF (Fig. 13b) samples. The highlighted regions 1 and 2 in the figure correspond to representative areas of short and long cracks. It can be seen that the shorter cracks (1) tend to form at triple junctions (TJs) and grain boundaries (GBs) regardless of any partial cycling. The longer cracks (2) appear to consist of short cracks at

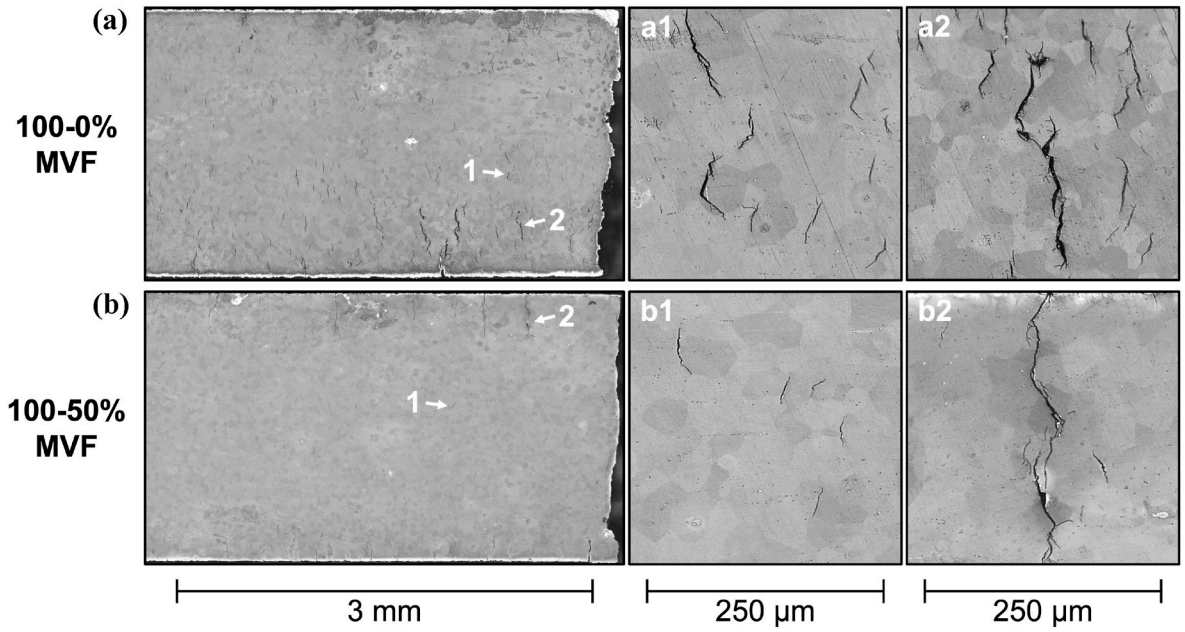

Fig. 13. Failed $Ni_{50.3}Ti_{29.7}Hf_{20}$ samples tested at 300 MPa to 100–0% MVF (a), and 100–50% MVF (b) polished and thermally etched to see how the surface cracks interact with the grains. Regions 1 and 2 marked with white arrows are zoomed in the mages to the right for each test condition. Region 1 shows a region of short cracks and region 2 is a region of long cracks where more crack propagation has taken place.

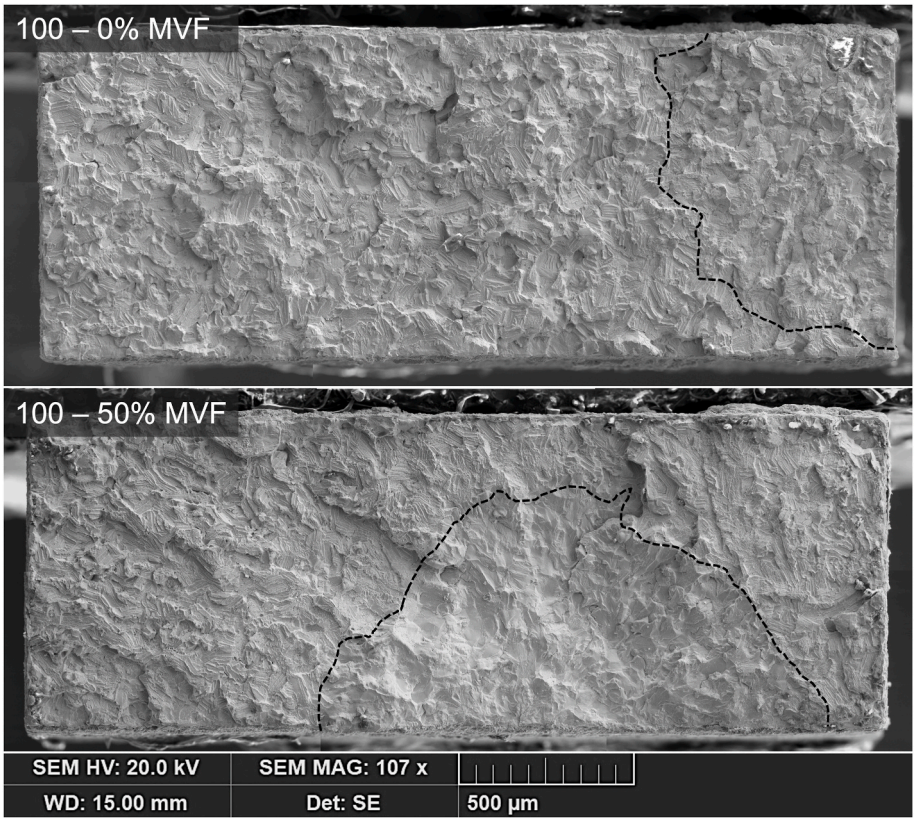

Fig. 14. Enlarged fracture surfaces of failed $Ni_{50.3}Ti_{29.7}Hf_{20}$ samples tested at 300 MPa to 100–0% MVF (a), and 100–50% MVF (b) to better display the differences in fracture surface characteristics between full and partial cycling. The edge of the crack propagation region before rupture is marked with a dashed black line. (a) The 100–0% MVF has a rougher surface with many sites of intergranular fracture between quasi-cleavage surfaces, even in the propagation zone. (b) The 100–50% MVF has a smoother fracture surface with some sites of intergranular fracture and quasi-cleavage in the rupture zone, but the propagation region is predominantly transgranular.

GBs and TJs connected mostly by transgranular cleavage. The difference between the fully and partially cycled samples is in how pervasive the short cracks are under the 100–0% MVF condition.

From the fracture surfaces (Fig. 9) larger crack propagation regions before rupture can be seen in samples undergoing less transformation. This is evidenced by the temper colors on the fracture surface where oxidation occurs at high temperatures during thermomechanical cycling. The 100–50% MVF sample had a crack propagation region covering ~33% of the surface area compared to only ~20% coverage in the 100–0% MVF sample. These greater regions of crack propagation imply a slower and more controlled crack growth regime emphasizing the observations made from the surface crack images. Additionally, Fig. 9 displays smooth cleavage fracture facets emanating from the crack initiation sites at the sample edge growing inward. Upon rupture the smooth facets roughen, and the crack appears to undergo quasi-cleavage which is consistent with previous observations of NiTi and NiTiHf fatigue fracture surfaces [34,35]. To better see the similarities and differences in these crack features a larger view of the fracture surfaces is displayed in Fig. 14. For ease of comparison only the fully transformed and 50% transformed samples are included, although the same trends were noticed across all four test conditions. The black dashed lines denote the transition from propagation to rupture zones. The intergranular features of the final failure region appear to be from microcrack nucleation and growth at GBs and TJs. These intergranular cracks are then connected by quasi-cleavage as these cracks start to span more than one or two grains. This was also observed in the surface crack images in Fig. 8.

The 100–0% MVF sample has a rougher failure surface overall, but especially in the propagation region, indicating more intergranular fracture throughout the sample as compared to 100–50% condition. This means there is significant damage accumulation at the grain interfaces of the fully transformed material. This localized damage is the result of dislocation accumulation at the GBs acting as stress risers and promoting crack nucleation. The 100–50% MVF sample also forms dislocations at GBs and TJs at the beginning of cycling, though not to the extent of the fully transformed sample. However, the transforming region likely shifts to different regions of the sample (especially the grain interiors) as new austenite/martensite, austenite/austenite, and martensite/martensite interfaces are inherently formed due to incomplete transformation providing additional sites for dislocation accumulation. This uniform oriented dislocation accumulation away from GBs and TJs prolongs the actuation fatigue lifetime by distributing damage accumulation away from these sites of high stress concentration reducing the driving force for crack nucleation. It is observed as a reduced amount of intergranular fracture.

4.3. Actuation fatigue mechanisms in partially cycled samples

The present results clearly demonstrate that partially cycling NiTiHf HTSMA samples between 100% martensite and a fraction of austenite during actuation results in longer fatigue lives. This is due to less transformation generating less extensive plastic deformation localization and less severe crack nucleation and propagation. These findings are consistent with the other partial cycle actuation fatigue studies in NiTi and NiTiCu SMAs mentioned earlier [13,21–23].

Understanding where martensitic transformation, and thus, accompanying plastic deformation is likely to occur during partial actuation cycling is one of the requirements to better understand the fatigue mechanisms responsible for the observed improvement in fatigue life. It has been reported that for bulk NiTiHf HTSMA samples, martensitic transformation occurs heterogeneously during full thermomechanical cycling in a precipitation hardened condition [36]. This heterogenous transformation is influenced by grain size, crystallographic orientation, and stress concentrations. Preferentially oriented grains and larger grains are most likely to transform first (decreasing grain size suppresses martensitic transformation) along with the areas of higher localized stress [37–40]. It is safe to assume that transformation induced damage would be restricted to these preferential transforming regions. If the material were then only partially cycled it would stand to reason that there would be an even sparser heterogenous distribution of transforming regions between different grains and within grains themselves. This would reduce the volume of material undergoing defect generation and damage. Belyaev et al. showed that the increase in defect density of partially heated NiTi SMAs was constrained only to the transforming volume [41].

In addition to the location of martensitic transformation in partially cycled samples, it is also necessary to understand the way damage is accumulated during actuation cycling. Šittner et al. performed extensive experimental and modelling studies on the plastic deformation accompanying martensitic transformation during actuation cycling. Among many findings, they determined that during reversible martensitic transformation under stress, dislocations mostly form in austenite (behind the habit plane) during reverse (martensite-to-austenite) transformation [42]. Martensite tends to nucleate nearer the center and spans across the grain, then grows laterally out to the edge of the grains, whereas austenite nucleates at opposing edges and grows toward the middle of the grain [43,44]. Thus, during heating cycles the grain centers will be the last to transform as the austenite forms from the edges.

To summarize the above discussion and literature results: (a) dislocation generation is localized to transforming regions, (b) dislocations form in austenite behind the habit plane during heating from martensite to austenite, and (c) the edges of grains undergo austenitic transformation before grain interiors. This is applicable to partial heating actuation fatigue because: (a) during partial cycling the transforming region evolves and so there is less severe dislocation accumulation, (b) there is less austenite per cycle under partial cycling meaning less dislocations are formed, and (c) austenite forming from grain edges promotes dislocation accumulation at high stress GBs and TJs under full cycling but is mitigated by the transformation regions shifting away from GBs and TJs during partial cycling. Additionally, there is a larger interfacial area between austenite and martensite (A-M), and between martensite variants (M-M) during full cycling as compared to partial cycling as the entire grain undergoes transformation when fully cycled. These interfaces, especially A-M, have been shown to have high local resolved shear stresses and slip systems can activate at these surfaces to relieve the stress [45–48]. These areas of high defect concentration are significant catalysts for crack nucleation. TEM investigations were attempted to visualize the dislocation structures present in fully and partially cycled samples. Unfortunately, room temperature imaging of martensite and in situ heating to austenite yielded no visible dislocations due to difficulties imaging defects in martensite, thin film effects and

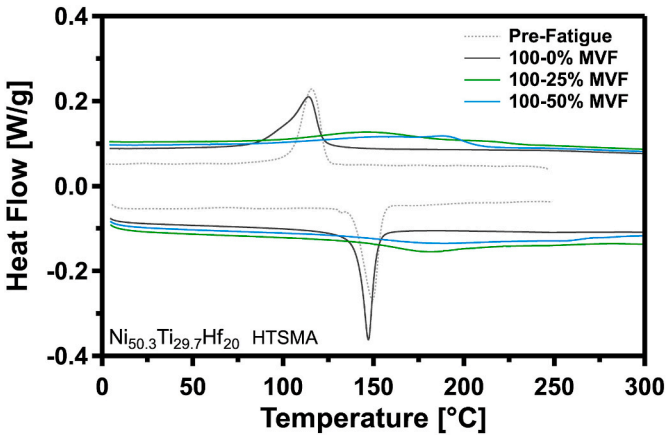

Fig. 15. DSC results of failed $Ni_{50.3}Ti_{29.7}Hf_{20}$ samples tested at 300 MPa to 100–0% MVF, 100–25% MVF, and 100–50% MVF compared to pre-fatigued material.

possible influences of Ga implantation during FIB lift out.

However, further evidence is presented by DSC results run on failed samples after actuation fatigue testing in Fig. 15. The austenite and martensite transformation peaks for the 100–25% MVF and 100–50% MVF samples are substantially broadened as would be expected from undergoing many actuation cycles. The widespread TRIP after so many cycles impedes transformation. This peak broadening is present in the 100–0% MVF but not as drastic as it survived an order of magnitude less thermomechanical cycles. There is very little change in transformation temperatures in the fully cycled sample as compared to the pre-fatigue condition. As the dislocations and damage are localized at the GBs and TJs so do not interfere much with the bulk transformation after only a couple of thousand cycles in this material. On the contrary, the transformation temperatures of the partially heated samples greatly increase, and the transformation range is broadened, due to high density dislocation accumulation heterogeneously (leading to broadening) and dislocation substructures resulting in oriented internal stress, and thus the increase in TTs.

5. Summary and conclusions

Actuation fatigue experiments were conducted on a nominal $Ni_{50.3}Ti_{29.7}Hf_{20}$ HTSMA to varying degrees of transformation under a fixed 300 MPa load. Fully cycled samples (100–0% MVF) were heated and cooled between a LCT of 45 °C (below M_f) and an UCT of 300 °C (above A_f). Partially cycled samples were run for 100 "control" cycles under full transformation (LCT to UCT) to move into a stable actuation regime and to determine the maximum achievable actuation strain. After the control cycles, the samples were heated from the LCT to a varying PHUCT until the desired fraction of maximum achievable actuation strain was obtained (90%, 75%, or 50%) and run to failure. Analysis of the fatigue data along with post-mortem analysis using SEM, fractography, TEM, and OM led to the following conclusions:

- Heating limited partial cycling significantly (more than an order of magnitude) increases the actuation fatigue lifetime in precipitation hardened $Ni_{50.3}Ti_{29.7}Hf_{20}$. The lower the degree of transformation the longer the lifetime. More importantly, partial thermal cycling and controlling actuation strain results in a much greater increase in fatigue life than lowering the actuation stress level, keeping the actuation work output same.
- Partial heating increases the actuation lifetime linearly with decreasing actuation strain under a constant force. The increase in lifetime with decreasing actuation strain due to a reduced load but maintaining a constant UCT is nonlinear.
- Partial heating reduces the amount of short crack nucleation during actuation fatigue and decreases crack propagation rate. Partial transformation promotes transgranular fracture in the crack initiation and propagation regimes, whereas full transformation largely undergoes intergranular crack propagation.
- Structural integrity is primarily undermined by the nucleation and growth of intergranular short cracks at grain boundaries and triple junctions. Long crack growth and rupture occurs predominantly by transgranular quasi-cleavage through grains bounded by intergranular short cracks regardless of full or partial cycling.
- Partial heating reduces crack initiation as transformation regions shift, dispersing dislocation and damage accumulation away from areas of high stress concentration, such as grain boundaries and triple junctions, extending actuation fatigue life.

CRediT authorship contribution statement

A. Demblon: Conceptualization, Methodology, Investigation, Writing – original draft, Writing – review & editing, Visualization. **J.H. Mabe:** Methodology, Investigation, Supervision, Funding acquisition, Resources. **I. Karaman:** Conceptualization, Methodology, Writing – review & editing, Validation, Supervision, Funding acquisition, Resources, Project administration.

Declaration of competing interest

The authors declare that they have no known competing financial interests or personal relationships that could have appeared to influence the work reported in this paper.

Data availability

Data will be made available on request.

Acknowledgements

The authors would like to acknowledge the financial support from the NASA University Leadership Initiative, under Grant No. NNX17AJ96A, and US National Science Foundation, Grant No. CMMI-1917367 and DMR-2004752. Use of the TAMU Materials Characterization Core Facility is acknowledged (RRID:SCR_022202) for SEM and TEM imaging. The authors would like to thank Professor Ruben Santamarta from the University of Ballearic Islands for his help on TEM analysis.

References

[1] G. Eggeler, E. Hornbogen, A. Yawny, A. Heckmann, M. Wagner, Structural and functional fatigue of NiTi shape memory alloys, Mater. Sci. Eng., A 378 (1) (2004/07/25/2004) 24–33, https://doi.org/10.1016/j.msea.2003.10.327.
[2] A. Demblon, et al., Compositional and microstructural sensitivity of the actuation fatigue response in NiTiHf high temperature shape memory alloys, Mater. Sci. Eng., A 838 (2022/03/24/2022), 142786, https://doi.org/10.1016/j.msea.2022.142786.
[3] O. Karakoc, et al., Role of microstructure on the actuation fatigue performance of Ni-Rich NiTiHf high temperature shape memory alloys, Acta Mater. 175 (2019) 107–120.
[4] A. Kreitcberg, V. Brailovski, S. Prokoshkin, Y. Facchinello, K. Inaekyan, S. Dubinskiy, Microstructure and functional fatigue of nanostructured Ti–50.26at% Ni alloy after thermomechanical treatment with warm rolling and intermediate annealing, Mater. Sci. Eng., A 562 (2013/02/01/2013) 118–127, https://doi.org/10.1016/j.msea.2012.11.013.
[5] B. Kockar, I. Karaman, A. Kulkarni, Y. Chumlyakov, I.V. Kireeva, Effect of severe ausforming via equal channel angular extrusion on the shape memory response of a NiTi alloy, J. Nucl. Mater. 361 (2–3) (2007) 298–305, https://doi.org/10.1016/j.jnucmat.2006.12.007.
[6] T. Umale, D. Salas, B. Tomes, R. Arroyave, I. Karaman, The effects of wide range of compositional changes on the martensitic transformation characteristics of NiTiHf shape memory alloys, Scripta Mater. 161 (2019/03/01/2019) 78–83, https://doi.org/10.1016/j.scriptamat.2018.10.008.
[7] J. Frenzel, E.P. George, A. Dlouhy, C. Somsen, M.-X. Wagner, G. Eggeler, Influence of Ni on martensitic phase transformations in NiTi shape memory alloys, Acta Mater. 58 (9) (2010) 3444–3458.
[8] J. Frenzel, A. Wieczorek, I. Opahle, B. Maaß, R. Drautz, G. Eggeler, On the effect of alloy composition on martensite start temperatures and latent heats in Ni–Ti-based shape memory alloys, Acta Mater. 90 (2015) 213–231.
[9] O. Benafan, G.S. Bigelow, A. Garg, R.D. Noebe, D.J. Gaydosh, R.B. Rogers, Processing and scalability of NiTiHf high-temperature shape memory alloys, Shape Mem. Superelast. (2021), https://doi.org/10.1007/s40830-020-00306-x.
[10] O. Karakoc, C. Hayrettin, D. Canadinc, I. Karaman, Role of applied stress level on the actuation fatigue behavior of NiTiHf high temperature shape memory alloys, Acta Mater. 153 (2018) 156–168.
[11] O. Karakoc, et al., Effects of upper cycle temperature on the actuation fatigue response of NiTiHf high temperature shape memory alloys, Acta Mater. 138 (2017) 185–197.
[12] O. Akgul, H.O. Tugrul, B. Kockar, Effect of the cooling rate on the thermal and thermomechanical behavior of NiTiHf high-temperature shape memory alloy, J. Mater. Res. 35 (12) (2020) 1572–1581, https://doi.org/10.1557/jmr.2020.139.
[13] G. Scirè Mammano, E. Dragoni, Effect of stress, heating rate, and degree of transformation on the functional fatigue of Ni-Ti shape memory wires, J. Mater. Eng. Perform. 24 (7) (2015) 2709–2719, https://doi.org/10.1007/s11665-015-1561-7.
[14] R. Casati, A. Tuissi, Effect of current pulses on fatigue of thin NiTi wires for shape memory actuators, J. Mater. Eng. Perform. 21 (12) (2012) 2633–2637, https://doi.org/10.1007/s11665-012-0281-5. Article.
[15] J. Frenzel, On the importance of structural and functional fatigue in shape memory technology, Shape Mem. Superelast. 6 (2) (2020/06/01 2020) 213–222, https://doi.org/10.1007/s40830-020-00281-3.

[16] M.M. Hasan, T. Baxevanis, Structural fatigue and fracture of shape memory alloy actuators: current status and perspectives, J. Intell. Mater. Syst. Struct. 33 (12) (2022/07/01 2021) 1475–1486, https://doi.org/10.1177/1045389X211057216.
[17] E. Hornbogen, Review Thermo-mechanical fatigue of shape memory alloys, Periodical (2004) 385–399. Available: https://search.ebscohost.com/login.aspx?direct=true&db=edsbl&AN=RN143064485&site=eds-live&scope=site&authtype=shib&custid=s8516548.
[18] M.J. Mahtabi, N. Shamsaei, M.R. Mitchell, Fatigue of Nitinol: the state-of-the-art and ongoing challenges, J. Mech. Behav. Biomed. Mater. 50 (2015/10/01/2015) 228–254, https://doi.org/10.1016/j.jmbbm.2015.06.010.
[19] K. Nargatti, S. Ahankari, Advances in enhancing structural and functional fatigue resistance of superelastic NiTi shape memory alloy: a Review, J. Intell. Mater. Syst. Struct. 33 (4) (2022/03/01 2021) 503–531, https://doi.org/10.1177/1045389X211023582.
[20] P. Shayanfard, et al., Stress raisers and fracture in shape memory alloys: review and ongoing challenges, Crit. Rev. Solid State Mater. Sci. 47 (4) (2022/07/04 2022) 461–519, https://doi.org/10.1080/10408436.2021.1896475.
[21] D.C. Lagoudas, D.A. Miller, L. Rong, P.K. Kumar, Thermomechanical fatigue of shape memory alloys, Smart Mater. Struct. 18 (8) (2009), https://doi.org/10.1088/0964-1726/18/8/085021.
[22] O.W. Bertacchini, D.C. Lagoudas, E. Patoor, Thermomechanical transformation fatigue of TiNiCu SMA actuators under a corrosive environment – Part I: experimental results, Int. J. Fatig. 31 (10) (2009) 1571–1578, https://doi.org/10.1016/j.ijfatigue.2009.04.012.
[23] M. Karhu, T. Lindroos, Long-term behaviour of binary Ti–49.7Ni (at.%) SMA actuators—the fatigue lives and evolution of strains on thermal cycling, Smart Mater. Struct. 19 (11) (2010), https://doi.org/10.1088/0964-1726/19/11/115019.
[24] S. Ganesan, S. Vedamanickam, Effect of operating parameters on functional fatigue characteristics of an Ni-Ti shape memory alloy on partial thermomechanical cycling, J. Intell. Mater. Syst. Struct. (2022), https://doi.org/10.1177/1045389x211072233.
[25] H.O. Tugrul, H.H. Saygili, B. Kockar, Influence of limiting the actuation strain on the functional fatigue behavior of Ni50.3Ti29.7Hf20 high temperature shape memory alloy, J. Intell. Mater. Syst. Struct. 32 (2) (2020) 219–227, https://doi.org/10.1177/1045389x20953610.
[26] A. Evirgen, "Microstructural Characterization and Shape Memory Response of Ni-Rich NiTiHf and NiTiZr High Temperature Shape Memory Alloys," Doctor of Philosophy, Texas A&M University, College Station, USA, 2014.
[27] A. Evirgen, I. Karaman, R. Santamarta, J. Pons, C. Hayrettin, R.D. Noebe, Relationship between crystallographic compatibility and thermal hysteresis in Ni-rich NiTiHf and NiTiZr high temperature shape memory alloys, in English, Acta Mater. 121 (Dec 2016) 374–383 [Online]. Available: <Go to ISI>://WOS:000386984500036.
[28] ASTM F2004-17 Standard Test Method for Transformation Temperature of Nickel-Titanium Alloys by Thermal Analysis, A. International, West Conshohocken, PA, 2017.
[29] M. Rahim, et al., Impurity levels and fatigue lives of pseudoelastic NiTi shape memory alloys, Acta Mater. 61 (10) (2013/06/01/2013) 3667–3686, https://doi.org/10.1016/j.actamat.2013.02.054.
[30] ASTM F2063-18 Standard Specification for Wrought Nickel-Titanium Shape Memory Alloys for Medical Devices and Surgical Implants, A. International, West Conshohocken, PA, 2018.
[31] P.K. Kumar, "Influence of Inelastic Phenomena on the Actuation Characteristics of High Temperature Shape Memory Alloys," Doctor of Philosophy, Texas A&M University, College Station, USA, 2009.
[32] M.C. Kuner, A.A. Karakalas, D.C. Lagoudas, ASMADA—a tool for automatic analysis of shape memory alloy thermal cycling data under constant stress, Smart Mater. Struct. 30 (12) (2021), 125003, https://doi.org/10.1088/1361-665x/ac2de2, 2021/10/25.
[33] K.C. Atli, I. Karaman, R.D. Noebe, D. Gaydosh, The effect of training on two-way shape memory effect of binary NiTi and NiTi based ternary high temperature shape memory alloys, Mater. Sci. Eng., A 560 (2013/01/10/2013) 653–666, https://doi.org/10.1016/j.msea.2012.10.009.
[34] B. Abut, B. Haghgouyan, I. Karaman, D.C. Lagoudas, Effect of specimen thickness on the fracture toughness of a NiTi shape memory alloy, Shape Mem. Superelast. 7 (1) (2021/03/01 2021) 90–100, https://doi.org/10.1007/s40830-021-00312-7.
[35] B. Haghgouyan, B. Young, S. Picak, T. Baxevanis, I. Karaman, D.C. Lagoudas, A unified description of mechanical and actuation fatigue crack growth in shape memory alloys, Acta Mater. 217 (2021), 117155, https://doi.org/10.1016/j.actamat.2021.117155, 2021/09/15/.
[36] W. Abuzaid, H. Sehitoglu, Functional fatigue of Ni50.3Ti25Hf24.7 – heterogeneities and evolution of local transformation strains, Mater. Sci. Eng., A 696 (2017) 482–492, https://doi.org/10.1016/j.msea.2017.04.097.
[37] X. Wang, C. Li, B. Verlinden, J. Van Humbeeck, Effect of grain size on aging microstructure as reflected in the transformation behavior of a low-temperature aged Ti–50.8at.% Ni alloy, Scripta Mater. 69 (7) (2013) 545–548, https://doi.org/10.1016/j.scriptamat.2013.06.023.
[38] X. Shi, et al., Grain size effect on the R-phase transformation of nanocrystalline NiTi shape memory alloys, J. Mater. Sci. 49 (13) (2014) 4643–4647, https://doi.org/10.1007/s10853-014-8167-6.
[39] F.M. Weafer, Y. Guo, M.S. Bruzzi, The effect of crystallographic texture on stress-induced martensitic transformation in NiTi: a computational analysis, J. Mech. Behav. Biomed. Mater. 53 (Jan 2016) 210–217, https://doi.org/10.1016/j.jmbbm.2015.08.023.
[40] G. Laplanche, T. Birk, S. Schneider, J. Frenzel, G. Eggeler, Effect of temperature and texture on the reorientation of martensite variants in NiTi shape memory alloys, Acta Mater. 127 (2017) 143–152, https://doi.org/10.1016/j.actamat.2017.01.023.
[41] S. Belyaev, N. Resnina, A. Sibirev, I. Lomakin, Variation in kinetics of martensitic transformation during partial thermal cycling of the TiNi alloy, Thermochim. Acta 582 (2014) 46–52, https://doi.org/10.1016/j.tca.2014.03.002.
[42] P. Šittner, et al., On the coupling between martensitic transformation and plasticity in NiTi: experiments and continuum based modelling, Prog. Mater. Sci. 98 (2018) 249–298, https://doi.org/10.1016/j.pmatsci.2018.07.003.
[43] B. Xu, G. Kang, C. Yu, Q. Kan, Phase field simulation on the grain size dependent super-elasticity and shape memory effect of nanocrystalline NiTi shape memory alloys, Int. J. Eng. Sci. 156 (2020), https://doi.org/10.1016/j.ijengsci.2020.103373.
[44] W.-S. Ko, B. Grabowski, J. Neugebauer, Impact of asymmetric martensite and austenite nucleation and growth behavior on the phase stability and hysteresis of freestanding shape-memory nanoparticles, Phys. Rev. Mater. 2 (3) (2018), https://doi.org/10.1103/PhysRevMaterials.2.030601.
[45] M.L. Bowers, X. Chen, M. De Graef, P.M. Anderson, M.J. Mills, Characterization and modeling of defects generated in pseudoelastically deformed NiTi microcrystals, Scripta Mater. 78–79 (2014/05/01/2014) 69–72, https://doi.org/10.1016/j.scriptamat.2014.02.001.
[46] D.M. Norfleet, et al., Transformation-induced plasticity during pseudoelastic deformation in Ni–Ti microcrystals, Acta Mater. 57 (12) (2009/07/01/2009) 3549–3561, https://doi.org/10.1016/j.actamat.2009.04.009.
[47] H.M. Paranjape, M.L. Bowers, M.J. Mills, P.M. Anderson, Mechanisms for phase transformation induced slip in shape memory alloy micro-crystals, Acta Mater. 132 (2017/06/15/2017) 444–454, https://doi.org/10.1016/j.actamat.2017.04.066.
[48] A.R. Pelton, G.H. Huang, P. Moine, R. Sinclair, Effects of thermal cycling on microstructure and properties in Nitinol, Mater. Sci. Eng., A 532 (2012) 130–138, https://doi.org/10.1016/j.msea.2011.10.073, 2012/01/15.